Feedback instability in the magnetosphere-ionosphere coupling system: Revisited

journal or publication title	Physics of Plasmas
volume	Vol.17
number	No.2
page range	pp.022904-1 - 022904-8
year	2010-02-01
URL	http://hdl.handle.net/10655/5379

doi: 10.1063/1.3304237

Physics of Plasmas

Feedback instability in the magnetosphere-ionosphere coupling system: Revisited

Cite as: Phys. Plasmas **17**, 022904 (2010); https://doi.org/10.1063/1.3304237
Submitted: 30 November 2009 • Accepted: 12 January 2010 • Published Online: 18 February 2010

T.-H. Watanabe

Feedback instability in the magnetosphere-ionosphere coupling system: Revisited

T.-H. Watanabe
National Institute for Fusion Science/The Graduate University for Advanced Studies, Toki, Gifu, 509-5292, Japan

(Received 30 November 2009; accepted 12 January 2010; published online 18 February 2010)

A coupled set of the reduced magnetohydrodynamic and the two-fluid equations is applied to the magnetosphere-ionosphere (M-I) feedback interactions in relation to growth of quite auroral arcs. A theoretical analysis revisiting the linear feedback instability reveals asymptotic behaviors of the dispersion relation and a non-Hermite property in the M-I coupling. A nonlinear simulation of the feedback instability in the M-I coupling system manifests growth of the Kelvin–Helmholtz-like mode in the magnetosphere as the secondary instability. The distorted vortex and field-aligned current profiles propagating as the shear Alfvén waves lead to spontaneous deformation of ionospheric density and current structures associated with auroral arcs. © *2010 American Institute of Physics*. [doi:10.1063/1.3304237]

I. INTRODUCTION

Auroral phenomena in polar regions are manifestations of complex interactions of the hot but low-density plasma in the magnetosphere and the cold but high-density plasma in the ionosphere.[1] A theory of quiet auroral arcs[2] based on the feedback interactions of the two media[3,4] explains that the ionospheric density and field-aligned current perturbations can spontaneously grow through the feedback instability. In the ionosphere with a large-scale perpendicular electric field, a density perturbation induces the small-scale polarization electric field, which propagates in the magnetosphere as the shear Alfvén waves carrying the field-aligned current. While the Alfvén waves are reflected back from the antihemisphere or at the magnetospheric equator, the ionospheric density perturbation slowly propagates across the field lines due to the Pedersen mobility. If the upward field-aligned current carried by the Alfvén wave coincides with the density enhancement, it amplifies the density perturbation as well as the field-aligned current and electric field fluctuations. This is the physical picture of the feedback instability in the magnetosphere-ionosphere (M-I) coupling system.

The two-dimensional simulation of the feedback instability was carried out by Miura and Sato with the assumption of the linear magnetohydrodynamic (MHD) response of the magnetosphere.[5] Then, three-dimensional MHD dynamics are taken into account in nonlinear simulations of the feedback instability[6,7] where global appearance of auroral arcs and effects of the field-aligned potential are investigated.[7]

The feedback instability has also been studied with regard to the ionospheric cavity modes in case with an inhomogeneous Alfvén speed profile along field lines.[8–10] The magnetospheric model has been extended to include two-fluid effects for an extremely low-density region,[11–13] and is applied to the subauroral zone as well.[14,15] A more elaborate simulation model of the feedback instability is developed to incorporate the nonlinearity of extended MHD equations, the dipole configuration, and the ionization processes.[16,17]

As briefly summarized above, physical and numerical models of the feedback instability have largely been advanced in the last three decades. Nevertheless, most of the analyses assume the linear magnetospheric response. Otherwise, the azimuthal symmetry or the elongated mode structure in the east-west direction is often presumed even in cases with the nonlinear (extended) MHD equations.[6,7,16,17] As will be discussed later, however, some of nonlinear terms breaking the azimuthal symmetry have the same order of magnitudes as those of the linear ones under the reduced MHD formalism,[18] and should lead to spontaneous deformation of auroral arcs in a nonlinear phase of the feedback instability.

In the present paper, we revisit the feedback instability analysis with the simplest physical settings, that is, the resistive MHD equations for the magnetosphere with straight field lines and the height-integrated model for the ionosphere. The M-I coupling model with nonlinear terms for the advection and the Lorentz force is constructed by means of the flute reduction for investigating the saturation process of the feedback instability. We believe that the nonlinear MHD effects should play important roles in auroral arc dynamics, such as splitting of arcs, curls, and spirals. To our knowledge, so far, nonlinear simulations of auroral arcs are limited to cases which start from initial conditions with well-developed arc structures, where the initial setup is unstable to the Kelvin–Helmholtz (K-H) instability causing deformation of arc structures (see, for example, Refs. 19 and 20). Nonlinear simulations of the feedback instability considered here would enable us to address growth and deformation of auroral arcs self-consistently and lead to deeper understandings of auroral arc dynamics.

This paper is organized as follows. We summarize derivation of a set of model equations for the M-I coupling system in Sec. II. In Sec. III, the linear feedback instability is reinvestigated, where we discuss the dispersion relation for normal modes, the asymmetric boundary conditions, the eigenfrequencies in the long and short wavelength limits, and the propagation angle dependence. Results of the nonlinear

simulation of feedback instability will be shown in Sec. IV where the numerical methods are also briefly described. A summary of the results is given in the last section.

II. MODEL EQUATIONS

A. Magnetospheric equations

For describing plasma dynamics in the magnetosphere, we consider the resistive MHD equations. The equation of motion and the Ohm's law are given as

$$\rho\left[\frac{\partial \boldsymbol{V}}{\partial t}+\boldsymbol{V}\cdot\nabla\boldsymbol{V}-\nu\left(\frac{1}{3}\nabla\nabla\cdot\boldsymbol{V}+\nabla^2\boldsymbol{V}\right)\right]=-\nabla p+\boldsymbol{J}\times\boldsymbol{B}, \tag{1}$$

$$\boldsymbol{E}=-\boldsymbol{V}\times\boldsymbol{B}+\eta\mathbf{J}, \tag{2}$$

where the current density $\boldsymbol{J}=\nabla\times\boldsymbol{B}/\mu_0$. The mass density and the permeability are denoted by ρ and μ_0, respectively. Other notations are standard. The continuity and energy equations will not be used in the following. In order to decouple the compressional Alfvén modes from the shear Alfvén one, we employ the flute reduction where an ordering procedure based on separation of the parallel and perpendicular scale lengths of perturbations is used to simplify the MHD equations.

Derivation of the reduced MHD equations is well established.[21] A smallness parameter $\epsilon\sim|k_\parallel/k_\perp|$ is introduced in a formal flute reduction of the MHD equations where $k_\parallel$ and $k_\perp$ mean wave numbers in the parallel and perpendicular directions to the magnetic field, respectively. Accordingly, the fast ($\boldsymbol{x}_f$) and slow ($\boldsymbol{x}_s$) spatial dependence of physical quantities are considered, such as $f(\boldsymbol{x}_f,\boldsymbol{x}_s,t)$. Thus, the spatial derivatives are evaluated both for the independent variables, $\boldsymbol{x}_f$ and $\boldsymbol{x}_s$,

$$\nabla=\frac{1}{\epsilon}\nabla_f+\nabla_s. \tag{3}$$

With the aim of applying the procedure to a general geometry in future works, we retain the expressions of $\boldsymbol{x}_f$ and $\boldsymbol{x}_s$ in this subsection after Ref. 21. Fluid and field variables are assumed to follow the ordering of

$$\begin{aligned}
\rho&=\rho_0(\boldsymbol{x}_s)+\epsilon\rho_1(\boldsymbol{x}_f,\boldsymbol{x}_s,t),\\
p&=p_0(\boldsymbol{x}_s)+\epsilon p_1(\boldsymbol{x}_f,\boldsymbol{x}_s,t),\\
\boldsymbol{V}&=\epsilon\boldsymbol{V}_0(\boldsymbol{x}_s)+\epsilon\boldsymbol{V}_1(\boldsymbol{x}_f,\boldsymbol{x}_s,t),\\
\boldsymbol{E}&=\epsilon\boldsymbol{E}_0(\boldsymbol{x}_s)+\epsilon\boldsymbol{E}_1(\boldsymbol{x}_f,\boldsymbol{x}_s,t),\\
\boldsymbol{B}&=\boldsymbol{B}_0(\boldsymbol{x}_s)+\epsilon\boldsymbol{B}_1(\boldsymbol{x}_f,\boldsymbol{x}_s,t).
\end{aligned} \tag{4}$$

The subscripts 0 and 1 mean equilibrium and perturbed quantities, respectively. Here, we explicitly keep the equilibrium flow perpendicular to $\boldsymbol{B}_0$ [as well as the corresponding electric field; $\sim O(\epsilon)$] while it is often absorbed in $\boldsymbol{V}_1$. The flow velocity is much slower than the shear Alfvén speed [$V_A=B_0/\sqrt{\mu_0\rho_0}\sim O(1)$]. The scalar and vector potentials are given as

$$\begin{aligned}
\Phi&=\epsilon B_0\phi_0(\boldsymbol{x}_s)+\epsilon^2B_0\phi(\boldsymbol{x}_f,\boldsymbol{x}_s,t),\\
\boldsymbol{A}&=\boldsymbol{A}_0(\boldsymbol{x}_s,t)+\epsilon^2[-\boldsymbol{B}_0\psi+\boldsymbol{A}_{\perp 1}(\boldsymbol{x}_f,\boldsymbol{x}_s,t)],
\end{aligned} \tag{5}$$

where $\boldsymbol{E}=-\nabla\Phi-\partial\boldsymbol{A}/\partial t$ and $\boldsymbol{B}=\nabla\times\boldsymbol{A}$. The dissipative coefficients, ν and η, are considered as $O(\epsilon^2)$ so that the leading order term such as $\nu\nabla_f^2\boldsymbol{V}$ remains in the order of ϵ. Here, $\boldsymbol{B}_0$ should satisfy $\nabla_s\times\boldsymbol{B}_0=0$. The parallel component of the current density is obtained from the Ampére's law,

$$J_\parallel=J_{\parallel 0}+\frac{B_0}{\mu_0}\nabla_f^2\psi, \tag{6}$$

where $J_{\parallel 0}=\boldsymbol{b}_0\times\nabla_s\times\boldsymbol{B}_0/\mu_0$.

The vorticity equation (the shear Alfvén law) is obtained by taking $\boldsymbol{b}\cdot\nabla\times$ of Eq. (1), where $\boldsymbol{b}=\boldsymbol{B}/B$, such that

$$\frac{\partial\omega}{\partial t}+\boldsymbol{V}_\perp\cdot\nabla_f\omega=V_A^2\nabla_\parallel\nabla_f^2\psi+\frac{2}{\rho_0}\boldsymbol{b}_0\times\boldsymbol{\kappa}_0\cdot\nabla_f p+\nu\nabla_f^2\omega. \tag{7}$$

Here, $\boldsymbol{b}_0$ is a unit vector parallel to $\boldsymbol{B}_0$, $\boldsymbol{V}=\boldsymbol{V}_\perp+V_\parallel\boldsymbol{b}_0$, $\omega=\boldsymbol{b}_0\cdot\nabla_f\times\boldsymbol{V}_\perp$, and $\boldsymbol{\kappa}_0=-\boldsymbol{b}_0\times(\nabla_s\times\boldsymbol{b}_0)$. The magnetic differential operator, $\nabla_\parallel$, is written as $\nabla_\parallel=\boldsymbol{b}_0\cdot\nabla_s+\{\psi,\}$, by neglecting $O(\epsilon)$ parts, where $\{,\}$ denotes the Poisson brackets defined by $\{\psi,\phi\}=\boldsymbol{b}_0\cdot\nabla_f\psi\times\nabla_f\phi$. The perpendicular velocity $\boldsymbol{V}_\perp$ is given by the perpendicular component of the Ohm's law. Thus, in the order of ϵ, one finds

$$\omega=\nabla_f^2\phi, \tag{8}$$

$$\boldsymbol{V}_\perp\cdot\nabla_f=\frac{\boldsymbol{E}_0\times\boldsymbol{B}_0}{B_0^2}\cdot\nabla_f+\{\phi,\}, \tag{9}$$

and $\nabla_f\cdot\boldsymbol{V}_\perp=0$. The parallel component of Eq. (2) describes the time evolution of ψ,

$$\frac{\partial\psi}{\partial t}+\frac{\boldsymbol{E}_0\times\boldsymbol{B}_0}{B_0^2}\cdot\nabla_f\psi=\frac{1}{B_0}\nabla_\parallel B_0\phi+\frac{\eta}{\mu_0}\nabla_f^2\psi, \tag{10}$$

where we ignore the resistive decay of the equilibrium magnetic field given by $-\partial\boldsymbol{A}_0/\partial t=\eta\boldsymbol{J}_0$ because of its slow evolution.

If the interchange term [the second term on the right hand side of Eq. (7)] is neglected, the pressure p is decoupled. Then, Eqs. (7)–(10) consist a closed set of the two-field reduced MHD equations. Here, the parallel components of the flow velocity and the perturbed magnetic field (as well as $\boldsymbol{A}_{\perp 1}$) are not included in the set of equations that describe the shear Alfvén dynamics.

B. Ionospheric equations

Ion and electron motions in the ionospheric E-layer are characterized by different ranges of frequencies (for example, see Ref. 22), such that

$$\tau^{-1}\ll\Omega_i\sim\nu_{ei}\ll\nu_{in}<\nu_{en}\ll\Omega_e. \tag{11}$$

Here, Ω_i and Ω_e mean the ion and electron (angular) cyclotron frequencies. In this section, the subscripts e, i, and n represent electron, ion, and neutral species, respectively. The electron-ion, ion-neutral, and electron-neutral collision fre-

quencies are, respectively, denoted by ν_{ei}, ν_{in}, and ν_{en}. Our concern here is the M-I coupling with slow time variations of the order of τ.

Collective motions of electrons in the ionosphere can be described by the drift kinetic approximation because of large Ω_e. By taking the zeroth order moment of the drift kinetic equation, the continuity equation for ionospheric electron density n_e is obtained as

$$\frac{\partial n_e}{\partial t} + \nabla_{\parallel}(n_e V_{e\parallel}) + \frac{\boldsymbol{E}\times\boldsymbol{B}}{B^2}\cdot\nabla n_e = S, \tag{12}$$

where S means a source and/or a sink term due to recombination and ionization. Height integration of Eq. (12) is often employed since the parallel wavelength of the shear Alfvén wave is considered to be much longer than the vertical thickness (h) of the ionosphere. By assuming that $\boldsymbol{B}$ and $\boldsymbol{E}$ accompanied with shear Alfvén waves are constant in the vertical direction in the ionosphere, one finds the height-integrated equation,

$$\frac{\partial \overline{n_e}}{\partial t} + \frac{\boldsymbol{E}\times\boldsymbol{B}_0}{B_0^2}\cdot\nabla_{\perp} n_e = \frac{J_{\parallel}}{eh} + \bar{S}, \tag{13}$$

where $\overline{\cdots}$ indicates the height average in the ionosphere. The operator $\nabla_{\perp}$ means the spatial derivative perpendicular to $\boldsymbol{B}_0$. For the $\boldsymbol{E}\times\boldsymbol{B}$ advection term in deriving Eq. (13), we have also employed the approximation of $(\boldsymbol{E}\times\boldsymbol{B}/B^2)\cdot\nabla \approx (\boldsymbol{E}\times\boldsymbol{B}_0/B_0^2)\cdot\nabla_{\perp}$, which is consistent with the flute reduction. The field-aligned current $J_{\parallel}$ is well approximated by $J_{\parallel}=-e\overline{n_e V_{e\parallel}}$ because of the small electron-ion mass ratio, $m_e/m_i \ll 1$.

The equation of motion for ions with the Krook collision term is written as

$$m_i n_i\left(\frac{\partial \boldsymbol{V}_i}{\partial t} + \boldsymbol{V}_i\cdot\nabla\boldsymbol{V}_i\right) = q_i n_i(\boldsymbol{E} + \boldsymbol{V}_i\times\boldsymbol{B}) - \nabla p_i - m_i n_i \nu_{in}\boldsymbol{V}_i, \tag{14}$$

where the flow velocity of the neutral atmosphere is assumed to be zero. The effective ion charge is denoted by q_i. The momentum loss of ions due to the ion-electron collision with recombination and/or ionization is also neglected. By the time-scale ordering in Eq. (11), one can omit the time derivative and Lorentz force terms in Eq. (14). The nonlinear advection term with the perpendicular scale length L can also be ignored in comparison to the neutral drag term, that is, $|\boldsymbol{V}_i|/\nu_{in}L \ll 1$, for typical ionospheric conditions. By assuming the isothermal condition, T_i=const., the ion number flux is given as

$$n_i\boldsymbol{V}_i = n_i\mu_P\boldsymbol{E} - D_i\nabla n_i, \tag{15}$$

where the (ion) Pedersen mobility $\mu_P = q_i/m_i\nu_{in}$ and the diffusion coefficient $D_i = T_i/m_i\nu_{in}$. Therefore, the height-integrated continuity equation for ions is given by

$$\frac{\partial \overline{n_i}}{\partial t} + \nabla_{\perp}\cdot(\mu_P\overline{n_i}\boldsymbol{E} - D_i\nabla\overline{n_i}) = \frac{e}{q_i}\bar{S}, \tag{16}$$

where we have also assumed the constant ν_{in} in the vertical direction.

In application to the auroral arc dynamics, it is appropriate to require the quasineutrality condition,

$$\overline{n_e} = \frac{q_i}{e}\overline{n_i} \equiv n, \tag{17}$$

because $\tau^{-1} \ll \omega_p$ and $L \gg \lambda_D$ where ω_p and λ_D are the plasma frequency and the Debye length, respectively. Thus, Eqs. (13) and (16) lead to

$$\frac{\partial n}{\partial t} + \frac{\boldsymbol{E}\times\boldsymbol{B}_0}{B_0^2}\cdot\nabla_{\perp} n = \frac{J_{\parallel}}{eh} + \bar{S}, \tag{18}$$

$$\nabla_{\perp}\cdot(\mu_P n\boldsymbol{E}) - \frac{\boldsymbol{E}\times\boldsymbol{B}_0}{B_0^2}\cdot\nabla_{\perp} n = D_i\nabla_{\perp}^2 n - \frac{J_{\parallel}}{eh}. \tag{19}$$

If one considers the recombination loss, the sink term may be given as $\bar{S}=-\alpha n^2$. In the present work, we employ a linearized recombination term, $\bar{S}=-2\alpha n_0\tilde{n}$, where $\tilde{n}$ denotes the perturbed ionospheric density from the background (n_0), $\tilde{n}=n-n_0$. In Eqs. (18) and (19), there are three unknowns, ϕ [where $\boldsymbol{E}=\boldsymbol{E}_0-\nabla_{\perp}(B_0\phi)$], n, and $J_{\parallel}$. In order to close the set of equations, thus, one needs to consider the M-I coupling. Introduction of the electron Pedersen mobility and/or the ion Hall mobility is straightforward but would have minor contributions because of the time-scale ordering in Eq. (11).

C. M-I coupling

According to the original work by Sato,[2] we employ the simplest M-I coupling model which consists of the uniform background magnetic field ($\boldsymbol{B}_0$) perpendicular to the height-integrated two-dimensional ionosphere. In this model, the ionosphere is coupled with the magnetosphere through the perpendicular electric field and the field-aligned current carried by the shear Alfvén waves. Hereafter, we use the Cartesian coordinates, where the z-axis is chosen to be parallel to the vertical equilibrium magnetic field. The ionosphere model of Eqs. (18) and (19) is solved in the x-y plane at $z=0$ by taking $\nabla_{\perp}=\hat{x}\partial/\partial x+\hat{y}\partial/\partial y$, where the hat $(\hat{\cdots})$ means the unit vector in the Cartesian coordinates. The equilibrium electric field, $\boldsymbol{E}_0$, is set in the y-direction by assuming the scalar potential $\phi_0(\boldsymbol{x}_s)=\phi_0(y)$. The fast and slow coordinates, $\boldsymbol{x}_f$ and $\boldsymbol{x}_s$, are chosen as $\boldsymbol{x}_f=(x\hat{x}+y\hat{y})/\epsilon$ and $\boldsymbol{x}_s=z\hat{z}+y\hat{y}$. Thus, $\boldsymbol{b}_0\cdot\nabla_s=\partial/\partial z$ and $\nabla_f=\nabla_{\perp}$. The y-dependence of $\boldsymbol{x}_s$ is involved so that $\boldsymbol{E}_0=-\hat{y}B_0\partial\phi_0/\partial y$. In the followings, we consider a case of the uniform equilibrium electric field, $\boldsymbol{E}_0=E_0\hat{y}$ with E_0=const.

In the equilibrium field of $\boldsymbol{B}_0=B_0\hat{z}$ with constant B_0, the magnetospheric equations are written as

$$\frac{D\omega}{Dt} + \{\phi,\omega\} = V_A^2\nabla_{\parallel}\chi + \nu\nabla_{\perp}^2\omega, \tag{20}$$

$$\frac{D\psi}{Dt} = \nabla_{\parallel}\phi + \frac{\eta}{\mu_0}\chi, \tag{21}$$

where the abbreviations are defined by

$$\omega = \nabla_\perp^2 \phi, \tag{22}$$

$$\chi = \nabla_\perp^2 \psi, \tag{23}$$

$$\frac{D}{Dt} = \frac{\partial}{\partial t} + \frac{\boldsymbol{E}_0 \times \boldsymbol{B}_0}{B_0^2} \cdot \nabla_\perp, \tag{24}$$

$$\nabla_\parallel = \frac{\partial}{\partial z} + \{\psi,\}, \tag{25}$$

$$\{\psi, \phi\} = \frac{\partial \psi}{\partial x}\frac{\partial \phi}{\partial y} - \frac{\partial \psi}{\partial y}\frac{\partial \phi}{\partial x}. \tag{26}$$

Since the interchange term vanishes due to $\boldsymbol{\kappa}_0=0$, the pressure is decoupled from Eq. (20). In the ideal case of $\nu=\eta=0$, Eqs. (20) and (21) have the same forms as those in a two-field limit of generalized reduced MHD equations.[23,24] From continuity of the electric field and the field-aligned current at $z=0$, we employ

$$\boldsymbol{E} = \boldsymbol{E}_0 - B_0 \nabla_\perp \phi, \tag{27}$$

$$J_\parallel = \frac{B_0}{\mu_0}\chi, \tag{28}$$

for solving Eqs. (18) and (19). These relations, thus, close the set of equations for the M-I coupling system.

D. Normalization

The governing equations are normalized by the horizontal (perpendicular) scale length L, the Alfvén speed V_A, and the magnetic field B_0, such that

$$\frac{\partial n}{\partial t} + \boldsymbol{E} \times \hat{z} \cdot \nabla_\perp n = J_\parallel - 2\alpha \tilde{n}, \tag{29}$$

$$\nabla_\perp \cdot (\mu_P n \boldsymbol{E}) - \boldsymbol{E} \times \hat{z} \cdot \nabla_\perp n = D_i \nabla_\perp^2 n - J_\parallel, \tag{30}$$

where $n=eh\mu_0 V_A n'/B_0$, $J_\parallel=\mu_0 L J_\parallel'/B_0$, $E=E'/B_0V_A$, $\mu_P=\mu_P' B_0$, and $\alpha=L\alpha' n_0'/V_A$. Prime $(\cdots')$ means a dimensional variable. Normalization of the reduced MHD equations, Eqs. (20) and (21), is trivial. Coordinate transformation from $(\boldsymbol{x}_\perp, z, t)$ to $(\boldsymbol{\xi}_\perp, z, t)$, where $\boldsymbol{\xi}_\perp = \boldsymbol{x}_\perp - \boldsymbol{E}_0 \times \hat{z}t$, eliminates the advection term for the equilibrium flow in Eqs. (24) and (29), while physical quantities such as $\boldsymbol{E}$ are supposed to be measured in the $\boldsymbol{x}_\perp$-frame. Here, we also assume homogeneous background ionospheric density (n_0=const). It is noted that the Hall ($\boldsymbol{E}\times\boldsymbol{B}$) drift motion of electrons with the mobility of $\mu_H=1/B_0$ (normalized to unity) is represented in the second term on the left hand side (l.h.s.) of Eq. (29). Since ions are assumed to be unmagnetized in the ionosphere [see Eq. (15)], the Hall current is carried by the $\boldsymbol{E}\times\boldsymbol{B}$ drift motion of electrons as shown in the second term on the l.h.s. of Eq. (30).

III. LINEAR ANALYSIS

In the ideal MHD limit ($\nu=\eta=0$), the linearized magnetospheric equations are reduced to the wave equations (normalized) for the shear Alfvén mode,

$$\partial_t \psi = \partial_z \phi \quad \text{and} \quad \partial_t \phi = \partial_z \psi. \tag{31}$$

The linearized version of Eqs. (29) and (30) is also given by

$$\partial_t \tilde{n} = J_\parallel - 2\alpha \tilde{n}, \tag{32}$$

$$-\mu_P n_0 \nabla_\perp^2 \phi + (\mu_P \boldsymbol{E}_0 - \boldsymbol{E}_0 \times \hat{z}) \cdot \nabla_\perp \tilde{n} = D_i \nabla_\perp^2 \tilde{n} - J_\parallel, \tag{33}$$

in the $(\boldsymbol{\xi}_\perp, z)$ coordinates.

We employ the periodic boundary condition in the $\boldsymbol{\xi}_\perp$-space for the perturbed quantities, and then, the linear solution for normal modes has a sinusoidal form of $\psi = \psi_{\boldsymbol{k}_\perp}(z)\exp(i\boldsymbol{k}_\perp \cdot \boldsymbol{\xi}_\perp - i\Omega t)$. Let us suppose an antisymmetric perturbation of $\psi_{\boldsymbol{k}_\perp}(z)$ with respect to the magnetospheric equator at $z=l$,

$$\psi_{\boldsymbol{k}_\perp}(z=l) = J_{\parallel \boldsymbol{k}_\perp}(z=l) = 0, \tag{34}$$

which implies the conjugate appearance of auroral arcs in the northern and southern hemispheres. (It is also straightforward to apply a symmetric boundary condition, $\partial_z \psi_{\boldsymbol{k}_\perp} = \partial_z J_{\parallel \boldsymbol{k}_\perp} = 0$ at $z=l$, while it does not alter the basic mechanism of the feedback instability.) Thus, the linear eigenfunction is obtained as

$$\psi_{\boldsymbol{k}_\perp}(z) = A[e^{ik_\parallel(z-l)} - e^{-ik_\parallel(z-l)}], \tag{35}$$

$$\phi_{\boldsymbol{k}_\perp}(z) = -A\frac{k_\parallel}{\Omega}[e^{ik_\parallel(z-l)} + e^{-ik_\parallel(z-l)}], \tag{36}$$

with an arbitrary constant A. Here, the dispersion relation of Eq. (31), $k_\parallel^2=\Omega^2$, demands $k_\parallel$ to be complex valued for growing or decaying solutions. From Eq. (31), one also finds the magnetospheric response at the ionosphere,

$$\left.\frac{\phi_{\boldsymbol{k}_\perp}}{J_{\parallel \boldsymbol{k}_\perp}}\right|_{z=0} = -\frac{k_\parallel}{\Omega k_\perp^2}\coth(ik_\parallel l) = -\frac{1}{k_\perp^2}\coth(ik_\parallel l). \tag{37}$$

Substituting Eq. (37) to Eqs. (32) and (33), one finds the dispersion relation in the $\boldsymbol{\xi}_\perp$-frame,

$$\Omega = \frac{\boldsymbol{k}_\perp \cdot [\mu_P \boldsymbol{E}_0 - \boldsymbol{E}_0 \times \hat{z}] - ik_\perp^2 D_i}{1 - \mu_P n_0 \coth(ik_\parallel l)} - 2i\alpha, \tag{38}$$

with $k_\parallel=\Omega$. The eigenfrequency in the $\boldsymbol{x}_\perp$-frame is obtained by replacing $\Omega|_{\boldsymbol{\xi}_\perp} \to \Omega|_{\boldsymbol{x}_\perp} - \boldsymbol{k}_\perp \cdot \boldsymbol{E}_0 \times \hat{z}$. If we rewrite $-\coth(ik_\parallel l)$ to $i\cot k_\parallel l$, Eq. (38) formally has the same expression as that obtained in Ref. 2, except for the collisional diffusion term for ions. However, $k_\parallel$ in Eq. (38) is complex valued, which means the amplitude of the shear-Alfvén wave varies along the field line, while $k_\parallel$ is taken to be real valued in the transmission line analysis employed in Ref. 2.

An equivalent representation to Eqs. (35) and (36), in terms of the upward and downward components of the shear Alfvén mode, clearly shows what the imaginary part of $k_\parallel$ means, such that $U=\psi-\phi$ and $D=-\psi-\phi$. Here, $U = U_{\boldsymbol{k}_\perp}(z)\exp(i\boldsymbol{k}_\perp \cdot \boldsymbol{\xi}_\perp - i\Omega t)$ and $D=D_{\boldsymbol{k}_\perp}(z)\exp(i\boldsymbol{k}_\perp \cdot \boldsymbol{\xi}_\perp - i\Omega t)$ with

$$U_{\boldsymbol{k}_\perp} = \psi_{\boldsymbol{k}_\perp} - \phi_{\boldsymbol{k}_\perp} = 2Ae^{ik_\parallel(z-l)}, \tag{39}$$

$$D_{\boldsymbol{k}_\perp} = -\psi_{\boldsymbol{k}_\perp} - \phi_{\boldsymbol{k}_\perp} = 2Ae^{-ik_\parallel(z-l)}, \tag{40}$$

for $k_\parallel=\Omega$. The upward and downward components satisfy $\partial_t U=-\partial_z U$ and $\partial_t D=\partial_z D$, respectively. Amplitude of the downward shear Alfvén wave is determined from that of the upward component launched from the ionosphere so as to satisfy the boundary condition at $z=l$, that is, $U_{\boldsymbol{k}_\perp}=D_{\boldsymbol{k}_\perp}$ or $U_{\boldsymbol{k}_\perp}=-D_{\boldsymbol{k}_\perp}$ (for the antisymmetric or symmetric conditions of $\psi_{\boldsymbol{k}_\perp}$, respectively). During the propagation of waves in the magnetosphere, the perturbation amplitude in the ionosphere varies in time for the decaying or growing solutions. Thus, the amplitudes of $U_{\boldsymbol{k}_\perp}$ and $D_{\boldsymbol{k}_\perp}$ change along the field line, which is described by the imaginary part of $k_\parallel$.

Now let us briefly discuss why the growing and decaying solutions of the shear Alfvén waves are allowed in the M-I coupling system even with the ideal MHD description for the magnetosphere. Equation (31) is rewritten into the ordinary differential equation for the shear Alfvén wave with the eigenfrequency Ω,

$$\mathcal{L}\psi_{\boldsymbol{k}_\perp} = \lambda_{\boldsymbol{k}_\perp}\psi_{\boldsymbol{k}_\perp}, \tag{41}$$

where the self-adjoint operator is given by

$$\mathcal{L}\psi = \frac{d}{dz}\left[p(z)\frac{d\psi}{dz} + q(z)\psi\right], \tag{42}$$

with $p(z)=1$, $q(z)=0$, and $\lambda_{\boldsymbol{k}_\perp}=-\Omega^2$. If the two arbitrary solutions of Eq. (41) defined on $a\le z\le b$, that is, $u(z)$ and $v(z)$, satisfy the boundary condition,

$$v^* p(z)\frac{du}{dz}\bigg|_{z=a} = v^* p(z)\frac{du}{dz}\bigg|_{z=b} \tag{43}$$

(where v^* means the complex conjugate of v), the Hermite condition

$$\int_a^b v^*\mathcal{L}u dz = \int_a^b u\mathcal{L}v^* dz \tag{44}$$

holds and the eigenvalues $\lambda_{\boldsymbol{k}_\perp}$ should be real (thus, the eigenfrequency Ω should be real or pure imaginary). In the M-I coupling system considered here, however, the boundary conditions of Eqs. (34) and (37) break the symmetry shown in Eq. (43) for $a=0$ and $b=l$, and the Hermite condition, Eq. (44), is not satisfied. Thus, the complex eigenvalues ($\lambda_{\boldsymbol{k}_\perp}$) and eigenfrequencies ($\Omega$) are allowed to exist. The same discussion can also be applied to cases with an inhomogeneous Alfvén velocity profile along field lines and a nonuniform background magnetic field.

Numerical solutions of the dispersion relation are shown in Figs. 1 and 2, where $l=10^3$, $E_0=10^{-3}$, $n_0=10$, $\mu_P=0.5$, $D_i=2\times10^{-5}$, and $\alpha=7\times10^{-4}$. Because of the coth (or cot) function in the dispersion relation, Ω is multivalued for a given $\boldsymbol{k}_\perp$. The lowest five solutions of Ω are plotted in Fig. 1 as functions of k_y for $k_x=0$, where $\boldsymbol{k}_\perp=k_x\hat{x}+k_y\hat{y}$. The feedback instability appears in a low k_y region, while the diffusion term stabilizes the higher k_y modes.

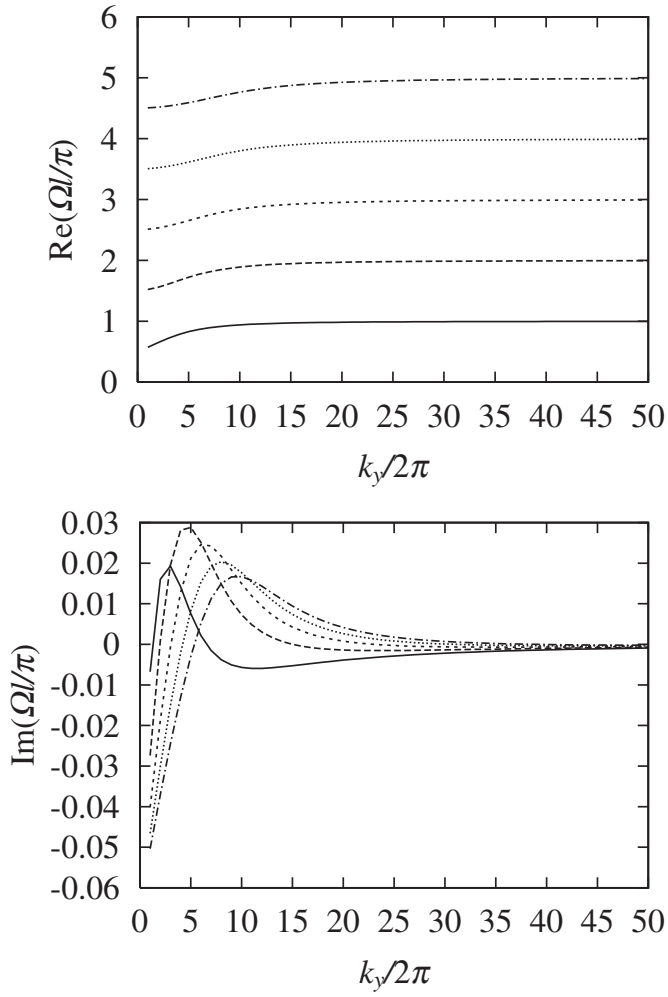

FIG. 1. Numerical solutions of the dispersion relation, Eq. (38), for $k_x=0$ modes, where $l=10^3$, $E_0=10^{-3}$, $n_0=10$, $\mu_P=0.5$, $D_i=2\times10^{-5}$, and $\alpha=7\times10^{-4}$.

It is meaningful to consider limiting behaviors of Ω for $|\boldsymbol{k}_\perp|\to\infty$ and $\boldsymbol{k}_\perp\to0$ [see Eqs. (23), (28), and (32)]. As $|\boldsymbol{k}_\perp|\to\infty$, $|J_\parallel(z)|$ as well as $|\vec{n}|$ is proportional to $k_\perp^2$ for a given amplitude (A) of ψ and ϕ. In order to satisfy Eq. (33) for $D_i=0$, however, $J_\parallel(z=0)$ should asymptotically approach zero so that the second term on the l.h.s will not diverge as $k_\perp^3$. It is accomplished by approaching $\cot\Omega l\to\infty$, that is, $\Omega l\to m\pi$ (where $m=1,2,\ldots$). This is nothing else but the field line resonance with nodes at the ionosphere and the magnetic equator. In contrast, Eq. (33) is approximated by $\mu_P n_0 k_\perp^2\phi\approx-J_\parallel+O(k_\perp^3)$ for $k_\perp\to0$. Substituting it into Eq. (37), thus, one finds $\cot\Omega l=i/\mu_P n_0$, which leads to $\mathrm{Re}(\Omega l)\approx(2m-1)\pi/2$ and $\mathrm{Im}(\Omega l)\approx-O(1/\mu_P n_0)$ for $|\mathrm{Re}(\Omega)|\gg|\mathrm{Im}(\Omega)|$. The limiting behaviors of Ω agree well with the numerical solutions shown in Fig. 1.

Linearly unstable solutions of Eq. (38) in the lowest branch of $\mathrm{Re}(\Omega)$ are presented in Fig. 2 by means of a contour plot of $\mathrm{Im}(\Omega l)$ in the k_x-k_y space for the same parameters employed in the above. The maximum growth rate is found near at $k_x=-4\pi$ and $k_y=2\pi$, that is, $\mathrm{Im}(\Omega l)\approx0.09\pi$. By taking a derivative of the dispersion relation for $\theta\equiv\tan^{-1}(k_y/k_x)$, one finds that the growth rate peaks at $\theta=-\tan^{-1}\mu_P$ for a given value of $k_\perp$. It means that the perpen-

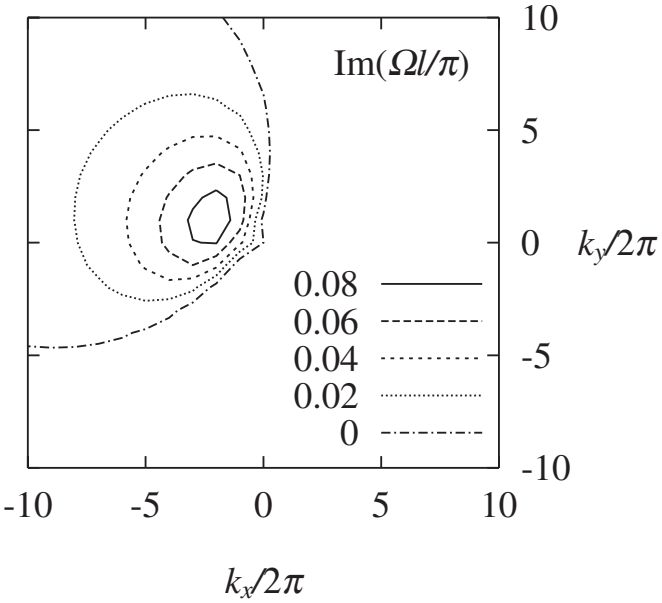

FIG. 2. Linear growth rate plotted in the $\boldsymbol{k}_\perp$-space for the same parameters as those used for the analysis shown in Fig. 1.

dicular wave number $\boldsymbol{k}_\perp$ providing the maximum growth rate is parallel to the ionospheric current given by a sum of the Pedersen and the Hall currents. (Here, the Hall mobility for electrons $\mu_H=1/B_0$ is normalized to unity.) The numerical result for $\mu_P=0.5$ shown in Fig. 2 agrees with the theoretical analysis. Although the most unstable mode is found for negative k_x, it propagates in the positive x (as well as in the positive y) direction in the $\boldsymbol{x}_\perp$-frame.

IV. NUMERICAL SIMULATION

We have carried out a nonlinear simulation of the feedback instability in the M-I coupling model described in Sec. II. The same parameters as those for the linear analysis are used but with finite dissipation, $\eta=\nu=4\times10^{-7}$. A sinusoidal perturbation of the linear eigenfunction with $(k_x,k_y)=(-4\pi,2\pi)$ in the lowest branch $(m=1)$ is given at $t=0$ as an initial seed for the instability growth. We set the perturbation amplitude of 10^{-5} for ψ and ϕ, which corresponds to that of 1.97×10^{-3} for ω and $J_\parallel$. Electrostatic potential perturbations with $(k_x,k_y)=(2\pi,-4\pi)$ and $(-2\pi,4\pi)$, having much smaller amplitude $(=10^{-7})$, are also added to the initial condition so as to trigger the secondary instability in a nonlinear stage of the primary one (the feedback instability).

The horizontal box size of the simulation domain discretized by numerical grids is normalized to unity both in the x and y directions. Employed are 256×256 grids in the x and y directions and 100 grids in the z direction. Spatial derivatives are evaluated by means of the fourth-order finite difference in a main part of the simulation domain, except at $z=0$, Δz, $l-\Delta z$, and l where the second-order finite difference is adopted. The grid size in the z direction is denoted by Δz. Numerical time integration is calculated by the fourth-order Runge–Kutta–Gill method. The time step size (which is set $\Delta t=4$ at $t=0$) is automatically changed so as to keep enough resolution.

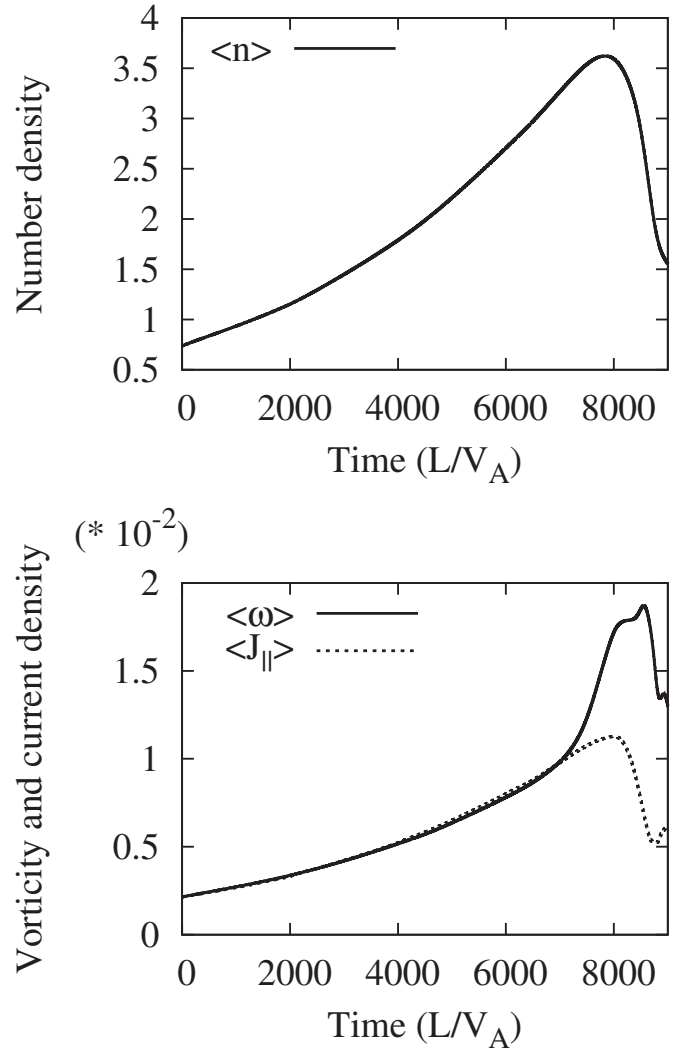

FIG. 3. Time histories of root-mean-square amplitudes (denoted by $\langle\cdots\rangle$) of the perturbed ionospheric density $\tilde{n}$ (top), the vorticity ω, and field aligned current $J_\parallel$ at $z=0$ (bottom) obtained by a nonlinear simulation of the feedback instability. The same parameters as those given in Fig. 1 are used but with $\eta=\nu=4\times10^{-7}$.

Time evolutions of root-mean-square amplitudes (denoted by $\langle\cdots\rangle$) of the ionospheric density, vorticity, and field-aligned current are shown in Fig. 3. The initially given perturbation with $(k_x,k_y)=(-4\pi,2\pi)$ linearly grows through the feedback instability. The peak amplitude of $\langle\tilde{n}\rangle$ exceeds 36% of the background density $(n_0=10)$ at $t\approx7700L/V_A$. The linear growth of the feedback instability characterized by $|\omega|\approx|J_\parallel|$ continues till $t\sim6000L/V_A$, and is followed by the nonlinear saturation.

A nonlinear development of the ionospheric density perturbation is presented in Fig. 4 by means of color contour plots at different time steps. At around $t\sim6000$ before saturation of the instability growth, the primary mode is faced with a nonlinear mode coupling. Then, the perturbations with higher mode numbers than that of the primary one grow through the nonlinearly induced secondary instability. At $t\sim8000L/V_A$, the striated mode structure of the density enhancement is torn into shorter filaments, which reminds us the splitting of auroral arcs.

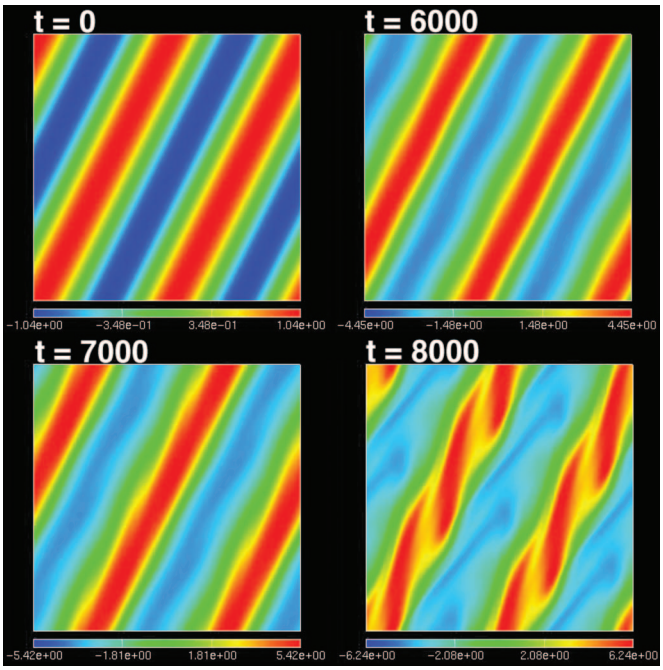

FIG. 4. (Color) Contours of ionospheric density perturbation ($\tilde{n}$) at different time steps of the nonlinear simulation.

Before the splitting of the density striation structure, the vorticity (ω) profile in the magnetosphere is largely distorted as shown in Fig. 5. Rolling-up of thin vortex sheets, which is typically seen in the K-H instability, is clearly found on the magnetic equator ($z=l$) at $t=7000L/V_A$, while the vorticity distribution on the ionosphere ($z=0$) exhibits a different pattern due to the strong inhomogeneity of the ionospheric conductivity. The equatorial vortex pattern becomes more turbulent at $t=8000L/V_A$. From the simulation results, therefore, it is concluded that the K-H-like secondary (nonlinear) instability is induced in the magnetosphere from the large-amplitude vortex sheets that have grown through the feedback instability. The deformation of the vortex and field-aligned current profiles caused by the K-H-like instability propagates as the shear Alfvén waves and leads to saturation of the ionospheric density increase.

V. SUMMARY

For studying the feedback interactions of the earth's M-I, we have formulated the three-dimensional slab M-I coupling model by means of the reduced MHD equations. The reduced MHD model is useful for describing the shear Alfvén waves with strongly anisotropic mode structure ($|k_\parallel/k_\perp| \ll 1$), and enables us to investigate fine structures of the ionospheric density and the field-aligned current perturbations associated with quite auroral arcs.

The dispersion relation for the normal modes of the feedback instability has the same form as that obtained in the original work by Sato[2] but with the complex-valued parallel wave number. The asymmetric boundary conditions at the ionosphere and the magnetospheric equator break the Hermite condition, and allow the complex eigenfrequencies of the shear Alfvén waves. Unstable eigenvalues are found in intermediate frequency ranges of $(m+1/2)\pi < \mathrm{Re}(\Omega l) < (m+1)\pi$ for the currentless condition at the magnetospheric equator, where $(m+1/2)\pi$ and $(m+1)\pi$ (field-line resonance) are asymptotic values of Ωl for $k_\perp \to 0$ and $k_\perp \to \infty$,

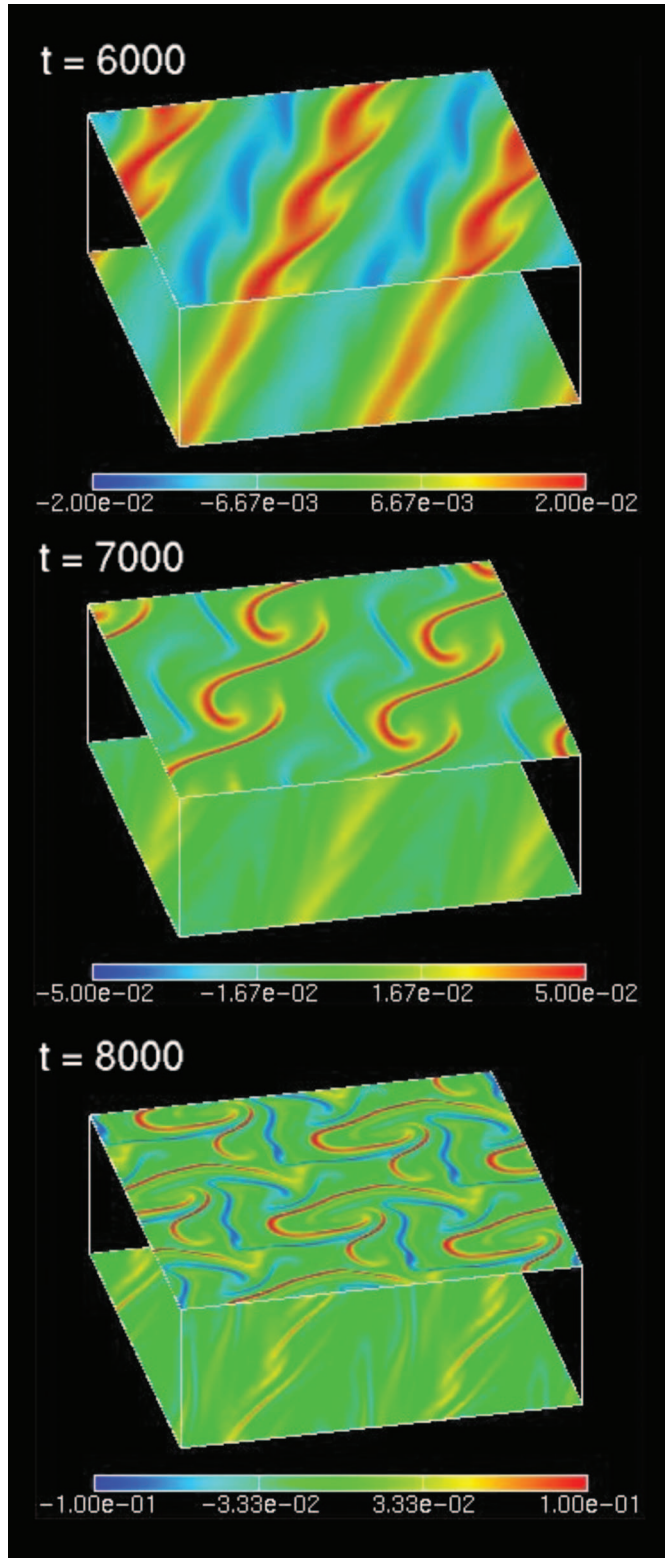

FIG. 5. (Color) Contours of the vorticity distributions on the ionosphere (lower plane) and the magnetic equator (upper plane) at three different time steps of the nonlinear simulation, where the vertical scale is shortened just for clarity of the plots.

respectively, and l denotes the field-line length from the ionosphere to the equator. For the same values of $k_\perp$, the maximum growth rate is found for $\boldsymbol{k}_\perp$ parallel to the ionospheric current.

By means of the reduced MHD equations, we derived the M-I coupling model with the nonlinear terms in the form of the Poisson brackets. A numerical simulation of the nonlinear evolution of the feedback instability is carried out, where saturation of the instability growth is observed. The K-H-like instability grows in the magnetosphere through the nonlinear coupling of the linearly stable and unstable modes. Then, splitting of striation structures of the ionospheric density is found, when growth of the ionospheric density and current perturbations is saturated. The present simulation demonstrates that nonlinear evolution of the feedback instability leads to structural changes of the density and field-aligned current patterns in the ionosphere. Although no brightening mechanism is taken into account in the present model, the obtained result suggests that the deformation of auroral arcs, such as splitting, curls, and spirals, could spontaneously appear during nonlinear development of the feedback instability in the M-I coupling system.

The M-I coupling model developed here has a simple slab configuration but can be straightforwardly extended to the dipole geometry. The linear analysis and nonlinear simulations of the feedback instability in the dipole magnetic field is currently in progress and will be reported elsewhere.

ACKNOWLEDGMENTS

Part of this work was completed when the author was an exchange scientist at the Institute for Fusion Studies, the University of Texas at Austin, under the Joint Institute for Fusion Theory, U.S.-Japan Fusion Cooperation Program. The author appreciates fruitful discussions with Professor W. Horton and Professor S. M. Mahajan during his stay at Austin, and deeply thanks Professor T. Sato for his continuous encouragements. This work is partly supported by NIFS/NINS under the project of Formation of International Network for Scientific Collaborations.

[1] Y. Kamide and W. Baumjohann, *Magnetosphere-ionosphere Coupling* (Springer-Verlag, Berlin, 1993), Chap. 2.
[2] T. Sato, J. Geophys. Res. **83**, 1042, doi:10.1029/JA083iA03p01042 (1978).
[3] G. Atkinson, J. Geophys. Res. **75**, 4746, doi:10.1029/JA075i025p04746 (1970).
[4] T. Sato and T. E. Holzer, J. Geophys. Res. **78**, 7314, doi:10.1029/JA078i031p07314 (1973).
[5] A. Miura and T. Sato, J. Geophys. Res. **85**, 73, doi:10.1029/JA085iA01p00073 (1980).
[6] K. Watanabe and T. Sato, Geophys. Res. Lett. **15**, 717, doi:10.1029/GL015i007p00717 (1988).
[7] T. Watanabe, H. Oya, K. Watanabe, and T. Sato, J. Geophys. Res. **98**, 21391 (1993); **99**, 6151, doi:10.1029/94JA00607 (1994).
[8] R. L. Lysak, J. Geophys. Res. **96**, 1553, doi:10.1029/90JA02154 (1991).
[9] O. A. Pokhotelov, D. Pokhotelov, A. Streltsov, V. Khrushev, and M. Parrot, J. Geophys. Res. **105**, 7737, doi:10.1029/1999JA900480 (2000).
[10] O. A. Pokhotelov, V. Khrushev, M. Parrot, S. Senchenkov, and V. P. Pavlenko, J. Geophys. Res. **106**, 25,813, doi:10.1029/2000JA000450 (2001).
[11] A. V. Streltsov and W. Lotko, J. Geophys. Res. **108**, 1289, doi:10.1029/2002JA009806 (2003).
[12] A. V. Streltsov and W. Lotko, J. Geophys. Res. **109**, A09214, doi:10.1029/2004JA010457 (2004).
[13] A. V. Streltsov and W. Lotko, J. Geophys. Res. **113**, A05212, doi:10.1029/2007JA012594 (2008).
[14] A. V. Streltsov and E. V. Mishin, J. Geophys. Res. **108**, 1332, doi:10.1029/2003JA009858 (2003).
[15] A. V. Streltsov and J. C. Foster, Phys. Plasmas **11**, 1260 (2004).
[16] J. Y. Lu, R. Rankin, R. Marchand, I. J. Rae, W. Wang, S. C. Solomon, and J. Lei, J. Geophys. Res. **112**, A10219, doi:10.1029/2006JA012195 (2007).
[17] J. Y. Lu, W. Wang, R. Rankin, R. Marchand, J. Lei, S. C. Solomon, I. J. Rae, J.-S. Wang, and G.-M. Le, J. Geophys. Res. **113**, A05206, doi:10.1029/2007JA012659 (2008).
[18] H. R. Strauss, Phys. Fluids **19**, 134 (1976).
[19] R. L. Lysak and Y. Song, J. Geophys. Res. **101**, 15,411, doi:10.1029/96JA00521 (1996).
[20] M. J. Keskinen and G. Ganguli, J. Geophys. Res. **101**, 26,995, doi:10.1029/96JA02175 (1996).
[21] R. D. Hazeltine and J. D. Meiss, *Plasma Confinement* (Addison-Wesley, Redwood City, 1992), Chap. 7.
[22] A. Hasegawa and T. Sato, *Space Plasma Physics 1 Stationary Processes* (Springer-Verlag, Berlin, 1989), Chap. 3.
[23] R. D. Hazeltine, C. T. Hsu, and P. J. Morrison, Phys. Fluids **30**, 3204 (1987) (see also references therein).
[24] V. M. Chmyrev, S. V. Bilichenko, O. A. Pokhotelov, V. M. Marchenko, V. I. Lazarev, A. V. Streltsov, and L. Stenflo, Phys. Scr. **38**, 841 (1988).